Coherent cross talk and parametric driving of matter-wave vortices

N. G. Parker,* A. J. Allen, C. F. Barenghi, and N. P. Proukakis
Joint Quantum Centre (JQC) Durham-Newcastle, School of Mathematics and Statistics, Newcastle University, Newcastle upon Tyne, NE1 7RU, United Kingdom
(Received 1 July 2012; published 20 July 2012)

We show that the interaction between vortices and sound waves in atomic Bose-Einstein condensates can be elucidated in a double-well trap: With one vortex in each well, the sound emitted by each precessing vortex can be driven into the opposing vortex (if of the same polarity). This cross talk leads to a periodic exchange of energy between the vortices which is long range and highly efficient. The increase in vortex energy (obtained by simulations of the Gross-Pitaevskii equation) is experimentally observable as a migration of the vortex to higher density over just a few precession periods. Similar effects can be controllably engineered by introducing a precessing localized obstacle into one well as an artificial generator of sound, thereby demonstrating the parametric driving of energy into a vortex.

DOI: 10.1103/PhysRevA.86.013631 PACS number(s): 03.75.Lm, 03.75.Kk

I. INTRODUCTION

In a quantum fluid, such as an atomic Bose-Einstein condensate (BEC) or superfluid helium, vortices possess quantized circulation, synonymous with them being a topological defect in the macroscopic phase of the underlying Bose-Einstein condensed component. Quantized vortices, vortex rings, vortex lattices, and vortex tangles have been the subject of experimental study in the context of superfluid helium for over 50 years [1], and in which recent emphasis has been on their role in quantum turbulence [2,3]. Meanwhile, since the late 1990s, there has been fast-growing interest in vortices in Bose-Einstein condensates [4,5], where the controllability and accessibility of these gases has led to the experimental generation of single vortices [6,7], giant vortices [8], vortex dipoles [9], soliton-vortex hybrids [10], and turbulent vortex tangles [11]. It is worthy of note that recent breakthroughs in imaging of both helium [12] and BEC [13] systems now enable the dynamics of quantized vortices to be monitored in real time.

The nature of the vortex-sound interaction in quantum fluids is far from clear [14]. The superfluid topology constrains quantized vortices to disappear only by annihilating with an oppositely charged vortex or by vanishing at the edge of the system (where they effectively annihilate with their image). In the limit of zero temperature and for a uniform condensate, sound waves are the low-lying excitations of the system and provide the only energy sink for vortex decay [15]. For example, at zero temperature the reconnection of vortex lines [17] and the acceleration of a vortex line segment both generate sound waves [18,19], dissipating the vortical excitation. In the latter case, the acceleration that drives sound emission may arise from the influence of velocity fields of other vortices [20,21], Kelvin-wave excitations of vortex lines [22,57–59], or the Magnus force arising from an inhomogeneous ambient density, for example, in a trapped condensate [23]. The experimentally observed decay of vorticity at very low temperature in superfluid He [24,25] is thought to be primarily due to the Kelvin-wave dissipation route, with reconnections playing only a secondary role [3].

Less well understood is the inverse process, that is, the absorption of sound by a quantized vortex. Insight may be gleaned from more general studies of vortex-sound interactions in fluid dynamics [14]. For example, an acoustic ray model has predicted that certain trajectories of sound wave can spiral into the core of a vortex filament, transferring energy into the vortical flow [26,27]. While sound waves can induce the nucleation of vortices through the collapse of cavitating bubbles [28,29], sound absorption by pre-existing vortices is not thought to play a significant role in homogeneous superfluid helium systems, for example, turbulent states, but may become considerable in atomic BECs due to their confined geometry. Indeed, the lack of sound-induced decay of a vortex precessing in a harmonically trapped BEC has been attributed to the reabsorption of the emitted sound by the vortex [23] (although related works [4,18] predict that the sound emission itself may be prohibited in a harmonic trap due to the sound wavelength exceeding the size of the system). The harmonic nature of the trap appears key to supporting a sound-vortex equilibrium, with trap anharmonicities inducing net vortex decay [23,30], in close analogy with dark solitons [31,32].

It is difficult to resolve and elucidate the interaction of sound with a vortex in single trapped condensate [21,23] due to their co-habitation in the trap. Furthermore, where multiple vortices exist in a system we may expect that they may interact via sound waves. However, within a single condensate, the interaction between vortices is dominated by the effect of their velocity fields. Such interaction is, for example, the dominant interaction mechanism in Tkachenko oscillations of a vortex lattice [54] and the dynamics of vortex dipoles [52,53], clusters [56], and arrays [57].

Here we will employ a double-well trap geometry to study the emission and absorption of sound between two vortices. With a low density channel between the wells and one vortex in each "subsystem," the velocity-induced vortex-vortex interaction is dramatically reduced but sound waves can still pass between the wells. By examining the dynamics of each vortex in their weakly connected subsystems, we may then infer the role of sound waves between vortices.

It is interesting to note that analogous questions exist over the acoustic properties of dark solitons. Like vortices, dark

*nick.parker@ncl.ac.uk

 ©2012 American Physical Society

solitons radiate sound waves under acceleration and become stabilized in harmonic traps [31,33]. The soliton-sound interaction was emphasized by the prediction of parametric pumping of sound into a dark soliton [20]. Moreover, a double-well geometry was recently shown to give insight into this interaction [34]: With one soliton in each well, a long-range sound-mediated interaction was evidenced by large-scale exchanges in energy between the solitons, controllable by the intertrap barrier.

The trap system and the theoretical model are outlined in Sec. II. In Sec. III we consider how a single vortex behaves in this double trap system. While these are not the main results of our work, it is an essential prerequisite to understanding the dynamics in later sections. In Sec. IV we progress to consider how two vortices, one in each well, "cross talk," that is, how they interact via the exchange of sound waves. In Sec. V we replace one of the vortices with a moving obstacle, and explore how the sound generated interacts with the remaining vortex. In Sec. VI we summarize and discuss our theoretical findings. In Sec. VII we demonstrate the same qualitative behavior in an experimentally achievable double trap geometry. Finally, in Sec. VIII we draw conclusions of our work.

II. THEORETICAL FRAMEWORK AND TRAP SETUP

We consider a BEC at ultracold temperatures such that thermal and quantum fluctuations can be neglected and that the system is well parametrized by a mean-field order parameter $\Psi(\mathbf{r},t)$ which satisfies the Gross-Pitaevskii equation (GPE) [35]. We assume a quasi-two-dimensional (quasi-2D) geometry, whereby harmonic trapping is sufficiently tight in one dimension, taken here to be the z direction, to freeze out the corresponding dynamics. Then, using the decomposition $\Psi(\mathbf{r},t) = \psi(x,y,t)\psi_z(z)$, one can integrate out the time-independent axial component $\psi_z(z)$ from the three-dimensional (3D) GPE. The transverse order parameter $\psi(x,y,t)$ then satisfies the 2D GPE,

$$i\hbar\partial_t\psi = \left(-\frac{\hbar^2}{2m}\nabla^2 + V(x,y) + g|\psi|^2 - \mu\right)\psi, \quad (1)$$

where $V(x,y)$ is the transverse trapping potential and m is the atomic mass. The 2D chemical potential μ is related to the 3D chemical potential μ' via $\mu = \mu' - \hbar\omega_z/2$, where ω_z is the trap frequency in the axial direction. s-wave atomic scattering, of length a, gives rise to the nonlinear term with coefficient $g = 2\sqrt{2\pi}\hbar^2 a/ml_z$, where $l_z = \sqrt{\hbar/m\omega_z}$ is the harmonic oscillator length of the frozen dimension.

The complex order parameter can be written as $\psi(x,y,t) = \sqrt{n(x,y,t)}\exp[i\phi(x,y,t)]$, where $n(x,y,t)$ and $\phi(x,y,t)$ are the distributions of atomic density and phase, respectively. Furthermore, the phase defines the fluid velocity $\mathbf{v} = (\hbar/m)\nabla\phi$. In 2D vortices are singular points about which the phase wraps around by an integer multiple of 2π and the condensate flows azimuthally. The density is pinned to zero at the central point creating a well-defined vortex core which relaxes to its unperturbed value at a distance of the order of the healing length $\xi = \hbar/\sqrt{mng}$.

We will initially consider an idealized double-well system consisting of two connected harmonic traps,

$$V(x,y) = \tfrac{1}{2}m\omega^2[(|x| - x_c)^2 + y^2]. \quad (2)$$

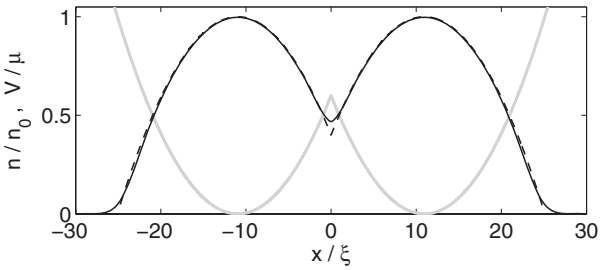

FIG. 1. Vortex-free density profile along the x axis (black solid line) in the double harmonic potential (gray solid line) with a barrier height at $x = 0$ of $V_0 = 0.6\mu$. The corresponding Thomas-Fermi profile $n_{\rm TF} = (\mu - V)/g$ is also shown (black dashed line).

Each trap is circularly symmetric with frequency ω and displaced from the origin by $\pm x_c$, as illustrated in Fig. 1. The barrier separating the trap, which has a minimum height of $V_0 = \frac{1}{2}m\omega^2 x_c^2$, determines the connectivity between the wells and thus the degree to which sound and vortices can propagate between wells. The transfer of sound waves, which have energy of order μ, between the wells will be possible for $V_0 < \mu$ and prohibited for $V_0 \gg \mu$. The capacity for vortices to propagate between wells will depend additionally on the energy of the vortex.

While this trap is not directly achievable in experiments due to its sharp feature at $x = 0$, it provides a convenient geometry to consider theoretically: It identifies the main physical effect in a "clean" manner and allows us to draw on the established knowledge of vortices in harmonic traps. After gaining understanding of the energy exchange processes, we will then demonstrate the same dynamics in experimentally achievable setups.

The 2D GPE is solved numerically using the Crank-Nicholson method [37]. Over the course of a typical simulation, the relative change in norm and energy $\Delta N/N$ and $\Delta E/E$ are of order 10^{-6}, that is, the solution is numerically well converged. The vortex-free ground state, with density profile $n_{\rm VF}(x,y)$, is found by propagating the 2D GPE in imaginary time. Vortices are further imposed by forcing the phase distribution during imaginary time propagation to

$$\phi(x,y) = \prod_i q_i \arctan\left(\frac{y - y_i}{x - x_i}\right), \quad (3)$$

where i is the index of a vortex with charge q_i located at (x_i, y_i). The converged state is then the condensate system with vortices at the desired locations. These are then propagated in real time according to Eq. (1). Note that since multiply charged vortices are energetically unfavorable compared to multiple singly charged vortices [1,35], we shall only consider singly charged vortices $|q_i| = 1$ (relative polarity may change). We will infer the change in energy of vortices in our system through changes in their position, for example, a drift to lower density signifies a decrease in the vortex energy. This is exactly what would be done in reality since vortex energy cannot be directly measured.

We assume units in which length, speed, and energy are expressed in terms of the 2D healing length $\xi = \hbar/\sqrt{mn_0 g}$,

speed of sound $c = \sqrt{n_0 g/m}$, and chemical potential $\mu = n_0 g$, where n_0 is the peak density.

The ratio $\mu/\hbar\omega$ specifies the nature of the condensate. For $\mu/\hbar\omega \ll 1$ the system is dominated by the trap and its ground state will approximate the Gaussian harmonic oscillator. For $\mu/\hbar\omega \gg 1$ the repulsive interactions dominate and lead to a broad condensate profile. Then the kinetic energy of the ground state, which depends on the gradient of the density, becomes sufficiently small that one can neglect it. Under this Thomas-Fermi (TF) approximation, the density profile has the analytic form $n_{\rm TF} = (\mu - V)/g$ [35]. We will focus on a system corresponding to $\mu/\hbar\omega = 10$. An example density profile for this system is shown in Fig. 1. The density is closely matched by the TF prediction, with the only significant deviation arising at the condensate perimeter and the barrier, where the variation in density becomes considerable. The physical effect of this is a smoothing of the density over a length scale of the order of the healing length. The TF approximation predicts that the harmonically trapped condensate extends up to a TF radius $R_{\rm TF} = \sqrt{2\mu/m\omega^2} = 14.14\xi$. While we hereafter express length in terms of healing length, this can be trivially related to the trap harmonic oscillator length $l_{\rm ho} = \sqrt{\hbar/m\omega}$ via $l_{\rm ho} = \sqrt{10}\xi$.

III. SINGLE VORTEX

We first explore the dynamics of a single vortex within the double trap system (2), initially placed in one well. A vortex tends to follow a path of equipotential through a trapped condensate, for example, precesses around the trap center in a single harmonic trap [38]. For our double trap system we can additionally anticipate a regime in which the vortex can traverse the interwell barrier and thus follow a dumbbell-shaped path around the system. As is well known for single harmonic traps, the energy and angular momentum associated with the vortex increases as the vortex is moved to higher density, that is, towards the centers of the well [4,35].

We place a vortex in the right-hand well at a position $(x_c, y_c + r_v)$, where $(x_c, y_c) = ([2V_0/m\omega^2]^{1/2}, 0)$ is the origin of the right-hand trap and r_v is the initial offset of the vortex from the well center. Note that the dynamics are not sensitive to the direction in which the vortex is initially off-set from the trap center; this is true throughout this work for all cases considered. The ensuing dynamics depend sensitively on the size of the vortex displacement r_v and the intertrap barrier V_0. We numerically evolve the vortex dynamics over a long simulation time $[5000(\xi/c)]$ within this parameter space. Note when the vortex initial position is very close to the edge of the cloud (typically within one healing length of $R_{\rm TF}$) its evolution becomes indistinguishable from the surface excitations that are generated and so we do not present results for such extreme positions.

The stability diagram for the dynamics of the vortex is plotted in Fig. 2, separating regions of "stable" vortex dynamics (dots) from those where there is no vortex within the system in the "final" simulated state (crosses), as discussed in detail below. Note that we observe a qualitatively similar stability diagram for a larger (more TF-like) condensate.

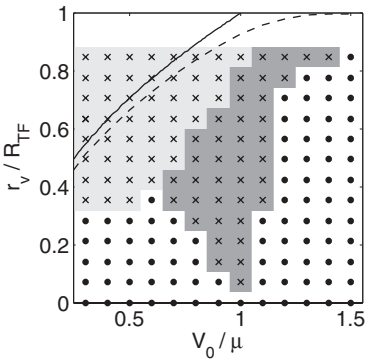

FIG. 2. Stability diagram in $r_v - V_0$ space for the single vortex case showing whether the final state [after a long simulation time of $5 \times 10^3(\xi/c)$] is a single vortex (dots) or the vortex-free state (crosses). The light-gray region is the crossover regime (case I), in which the vortex passes into the far well. The dark-shaded region is the inductive regime (case II), in which the initial vortex induces other vortices. The lines are the TF predictions for the onset of crossover dynamics $r_v/R_{\rm TF} = \sqrt{(1 - n_{\rm min}/n_0)}$ using the TF prediction (solid line) and the numerical values (dashed line) for $n_{\rm min}$. The TF radius of each well is $R_{\rm TF} = 14.14\xi$.

A. Stable dynamics

If the vortex excitation was stable and free from decay [36], we would expect the vortex to always remain in the system. In Fig. 2 we see regimes where this is true (dots) but also where the vortex is unstable and ultimately leaves the system (crosses). Stable vortex motion is promoted for large V_0, since the well then behaves likes an isolated harmonic trap, and for low vortex radii, since the vortex does not feel a strong effect from the far trap. Under this stable motion the vortex dynamics is akin to that in a single harmonic trap [23]: it precesses around the well center with an approximately constant radius and generates a collective motion of the background condensate of low amplitude ($\sim 5\% n_0$). In Fig. 3 we show a typical snapshot of the condensate. The density distribution consists of two weakly connected circular condensates and the vortex appears as a hole (white spot) in the right-hand well. By subtracting the time-independent vortex-free density $n_{\rm VF}$ from this density profile, the collective excitations become clearly visible [Fig. 3(b)]. The precession frequency of the vortex is $\sim 0.2\omega$ for small displacements, and increases with r_v, in good agreement with analytic predictions for vortex precession in a single harmonic trap in the TF regime [39].

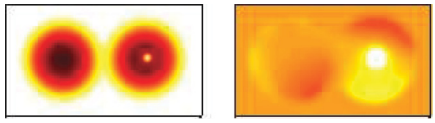

FIG. 3. (Color online) (Left) Density $n(x, y)$ for the single vortex scenario with $y_v = 1\xi$ and $V_0 = 0.9\mu$ at a time of 1000 ξ/c. Black (white) corresponds to peak (zero) density. (Right) Renormalized density $n(x, y) - n_{\rm VF}(x, y)$ for the same data as above. The color scale is $\pm 10\% n_0$. Each box is of size $64\xi \times 32\xi$.

B. Unstable dynamics

In cases where the vortex eventually decays from the system (crosses in Fig. 2) its initial dynamics falls into one of two cases. In case I, the dynamics is characterized by the vortex *crossing over* into the adjacent well, whereas in case II it is characterized by *inducing* a mirror vortex in the adjacent well. These effects most commonly become manifested in the first precession of the vortex in the trap, but in a minority of cases they may arise after several precessions.

1. Case I: vortex crossover

Case I (vortex crossover) arises in the lightly shaded region in Fig. 2. The vortex can be expected to travel between the wells when the local potential of the vortex (the value of the potential at the vortex core) exceeds the interwell barrier. This will tend to occur for large vortex offsets and a weak intertrap barrier, as in qualitative agreement with the position of this region in Fig. 2. Put quantitatively, one would expect crossover to occur when the vortex density depth n_v is less than or equal to the minimum density at the barrier $n_{\rm min}$ (one can picture this as when the vortex can just squeeze through the barrier). If decayless, the density depth of the vortex will retain its initial value, which we can approximate via the TF prediction $n_v = n_0(1 - r_v^2/R^2)$. This is a robust approximation provided that the vortex position is away from the edge and the barrier, for which the TF density agrees with the actual density profile to within $0.01n_0$. This gives the criteria $r_v/R \geqslant \sqrt{1 - n_{\rm min}/n_0}$ for crossover to be possible. We can first approximate $n_{\rm min}$ via its TF prediction $n_{\rm min}^{\rm TF} = n_0(1 - V_0/\mu)$, giving the solid line. However, the onset of crossover dynamics occurs at considerably lower r_v. We can expect some deviation to arise from the inaccuracy of using the TF approximation for $n_{\rm min}$: The TF approximation underestimates the density at the point of the barrier, as evident in Fig. 1.

If we instead use the actual value of the ground-state density at the barrier, we obtain the threshold shown by the dashed line in Fig. 2. This lowers the prediction for r_v, but only slightly and the prediction still remains considerably greater than the observed threshold. This anomaly is likely to arise from the fact that the vortex radiates sound during its motion and thereby drifts to lower densities and greater radial position.

In this crossover regime, the ultimate fate of the vortex is to decay. In Fig. 4 we present an example. The precessing vortex approaches the barrier [$t = 30(\xi/c)$] and upon traversing it [$t = 60(\xi/c)$], decays into a high-amplitude curved pulse of sound [$t = 67.5(\xi/c)$]. The sound pulse reflects off the far left side of the trap and propagates back through the trap [$t = 120(\xi/c)$]. Following many reflections and diffractions in the trap, the sound pulse becomes randomized, ultimately forming an isotropic sound field [$t = 375(\xi/c)$].

In other cases, the vortex undergoes a more gradual decay, passing many times between the wells. *Nota bene* more generally, we can observe some cases where the vortex undergoes stable crossover dynamics, as we will see later in Sec. VII.

2. Case II: vortex induction

The second case of unstable dynamics (case II, vortex induction), characterized by the initial vortex inducing a second vortex in the far well, arises in the dark shaded region in Fig. 2. Snapshots of a typical evolution are shown in Fig. 5. As the vortex precesses close to the adjoining well ($t = 300\xi/c$), a mirror vortex becomes excited on the opposite side of the interwell barrier. This vortex has the opposite charge to the original vortex and precesses in the opposite direction around its trap ($t = 415\xi/c$). This early induction is the characteristic of this regime of dynamics. The subsequent dynamics can vary widely. In the example, the initially induced vortex disappears ($t = 500\xi/c$), a second vortex is induced ($t = 720\xi/c$), and then the original right-hand vortex disappears ($t = 920\xi/c$). In other cases the original vortex may disappear as it creates its mirror vortex, while sometimes the induced vortex may itself induce a vortex in the right-hand well. As a result there can arise periods of time where multiple vortices can appear in the system. For all cases we observe the growth of a tempestuous sound field during the vortex motion, set up by the sound emission from the accelerating vortices. All of the vortices ultimately dissipate and disappear into an energetic and isotropic sound field [Fig. 5(b) at $t = 1540\xi/c$].

Up until the point when it disappears, the original vortex drifts outwards, as shown in Fig. 5(b). Most of the noise in $r_v(t)$ is due to the buffeting effect that the sound field has on the vortex. However, the sizable jumps in r_v at $t \sim 300$ and $700(\xi/c)$ (highlighted by arrows) occur as a vortex is induced in the far well, indicating the transfer of energy from the original vortex to create the new one.

This region of the parameter space occurs for a range of barrier heights in the vicinity of $V_0 = \mu$, for which the condensate channel is of low density. The energy to create a

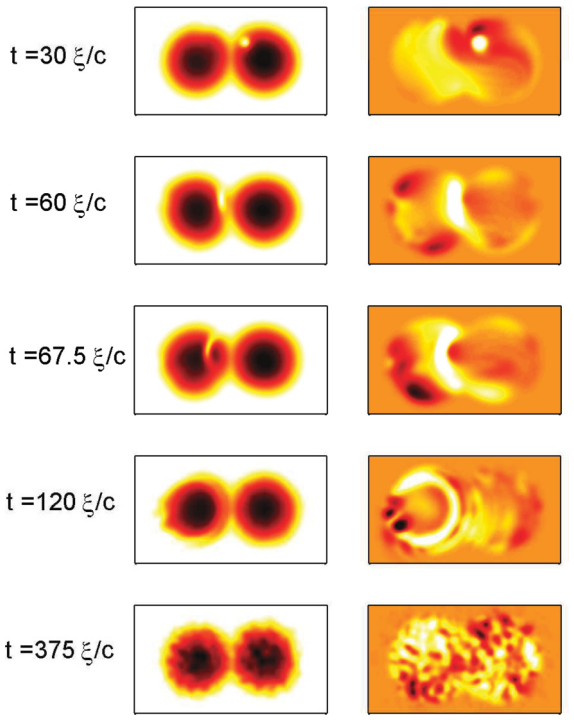

FIG. 4. (Color online) Crossover regime dynamics as follows: snapshots of (left) density $n(x,y)$ and (right) renormalized density $n(x,y) - n_{\rm VF}(x,y)$ within the crossover regime, for $r_v = 8\xi$ and $V_0 = 0.6\mu$, at various times. (Spatial and color scales are the same as in Fig. 3).

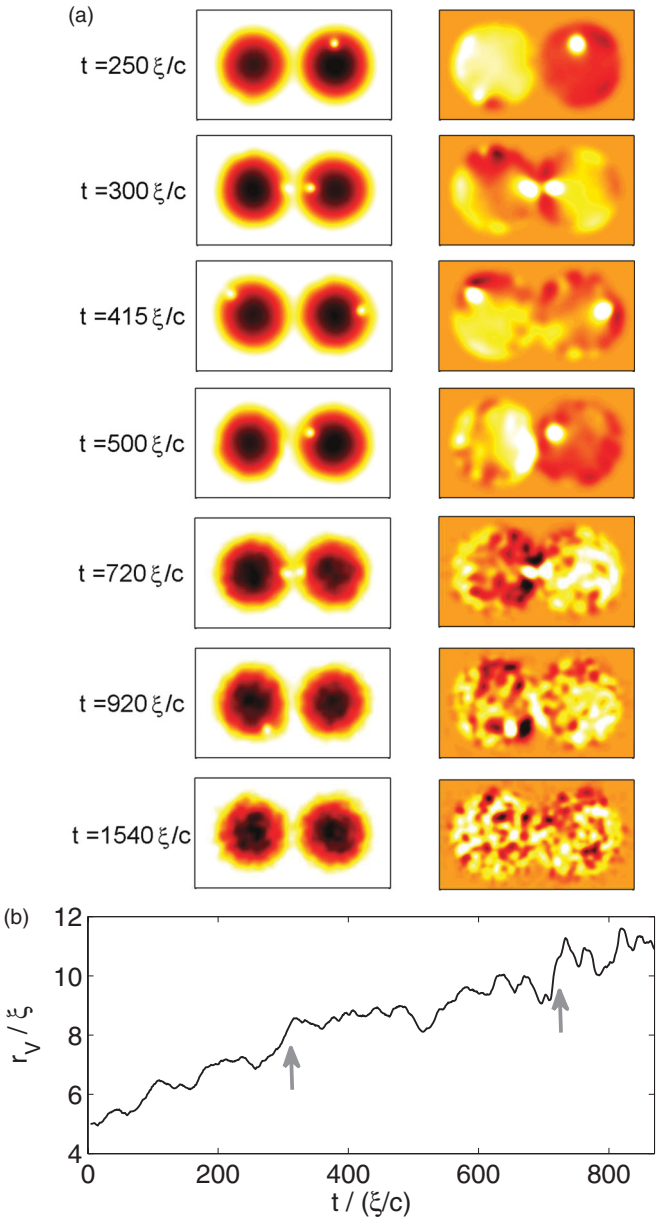

FIG. 5. (Color online) Inductive regime dynamics as follows: (a) density $n(x,y)$ (left column) and renormalized density $n(x,y) - n_{\mathrm{VF}}(x,y)$ (right column) at various times. Parameters are as follows: $r_v = 5\xi$ and $V_0 = 0.9\mu$ (box size and color scale are the same as in Fig. 3). (b) Evolution of the radial position of the vortex r_v; arrows indicate the points at which vortex induction takes place.

vortex depends on the local density. As the barrier height is reduced below μ, the density in the barrier region increases and we have confirmed with numerical simulations that the energy cost to create a vortex here increases sharply.

IV. CROSS TALK OF TWO VORTICES

We now extend to the case where there is initially a vortex in *each* well to examine the possibility of sound-induced interaction between vortices, in analogy to the dark soliton setup of Ref. [34]. We continue to employ the idealized double harmonic trap geometry; we will demonstrate the same phenomena in a realizable double trap geometry in Sec. VII. The additional vortex (denoted "vortex 2") is created at the center of the left-hand trap. Note that since it feels the velocity field of vortex 1 it will not be perfectly stationary. The displacement of vortex 1, denoted r_v, and the height of the interwell barrier V_0, are again key to the dynamics. The latter parameter now additionally controls the transfer of sound between the wells, since sound waves have an energy of around μ. We can also expect sensitivity to the relative polarity of the vortices. Figure 6 shows the stability diagram of the system for (a) vortices of the same polarity and (b) vortices of opposite polarity.

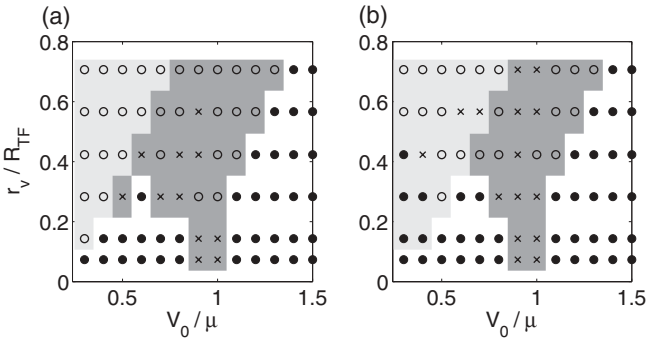

FIG. 6. Stability diagram in $r_v - V_0$ of the final state [after $5000(\xi/c)$] of the two vortex systems for (a) same polarity and (b) opposite polarity of the vortices. The final state is either two stable vortices (solid circles), one stable vortex (open circles), or no vortices (crosses). The second vortex is initially positioned at the center of the left-hand well. Light and dark shading indicates case I (crossover) and case II (induction) of the unstable dynamics.

The stability diagrams are somewhat similar to that of the single vortex case (Fig. 2) and the vortex polarity only has a small effect on the final state of the system. There are two stable regions, one for weak barriers and low displacements, and the other for large barriers. We also see a crossover regime for weak barriers and large vortex displacements in which vortex 1 tends to cross into the other well, and an induction regime for barrier heights centered around μ in which vortex 1 induces another vortex in the opposite well. Where vortex instability does occur, the end state is either the persistence of a single vortex or no vortices at all. We cannot make any general comments about what favors these two end states: The dynamics that can develop are sufficiently complex, for example, featuring vortex crossover and induction, and interaction with sound waves and collective condensate modes, that the end state is not readily deterministic. However, the most important information carried by these plots is simply whether or not the two-vortex state remains stable (irrespective of what the outcome of an instability actually is in terms of the number of vortices left).

Note that in Fig. 6(b) there exists stable dynamics in the crossover regime. In this case vortex 1 perpetually traverses both wells in a stable manner while vortex 2 remains localized in the center of its well.

In order to investigate the cross talk between vortices, that is, their sound-mediated interactions, we focus on the stable regimes and in particular the stable area occurring for low barrier heights, for which we can expect unimpeded motion of

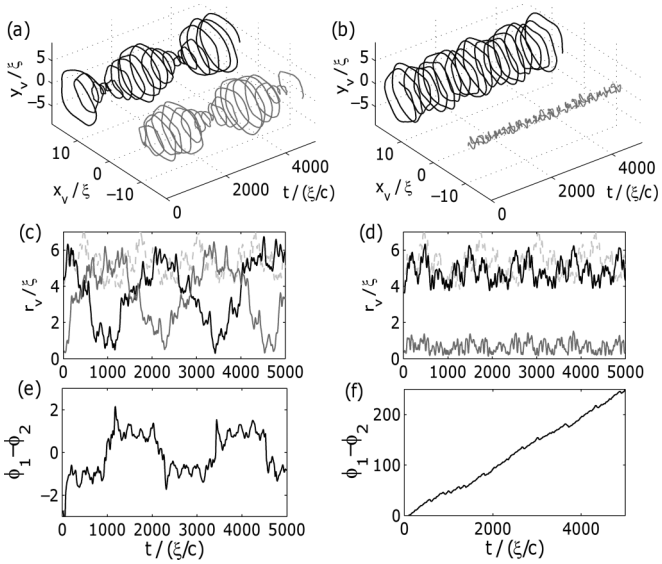

FIG. 7. Vortex dynamics in the two-vortex system with (a) the same polarity and (b) different polarity. Parameters are as follows: $r_1(t=0)=4\xi$, $V_0=0.6\mu$. Black (gray) lines correspond to vortex 1 (2). (c) and (d) Plot of the corresponding vortex radii, and additionally including the evolution of a single vortex in the double trap (gray dashed line) with initial radius $r_v(t=0)=4\xi$. (e) and (f) Plot of the corresponding phase difference between the two vortices.

sound between the wells. Figure 7 presents the vortex dynamics for $r_v = 4\xi = 0.28R_{\rm TF}$ and $V_0 = 0.6\mu$. When the vortices have the same charge [Fig. 7(a)] the vortices periodically spiral inwards and outwards, and remain out of phase with each other. The change in the vortex radial position [Fig. 7(c)] is large (the vortices oscillate between the trap center and a radius of around $6\xi = 0.43R_{\rm TF}$), demonstrating a significant transfer of energy between the vortices. The energy exchange occurs over a time scale of $\sim 2000(\xi/c)$, which is around eight precessions of the vortex in the trap [the precession period is $\sim 270(\xi/c)$]. In the analogous situation for the dark soliton, the energy transfer is much slower, occurring over many tens of soliton oscillations [34].

When the vortices have opposing polarity [Figs. 7(b) and 7(d)], no significant transfer of energy is observed between the vortices. The vortices are observed to precess with an approximately constant radius. The vortex motion does undergo significant modulations which arise from the back-action of the randomized sound field on the vortices. Such modulations do not arise from vortex-vortex coupling as they are also observed for a single vortex in the double well [gray dashed line in Fig. 7(d)].

The significant transfer of energy between like-charged vortices and insignificant transfer between unlike-charged vortices is consistent across the stable region of the parameter space at low barrier heights. For high V_0 we do not observe energy transfer since the transfer of sound across the barrier becomes prohibited.

Further insight into the transfer of energy can be gleaned by considering the phase difference between the trajectories of the vortices $\phi_1 - \phi_2$, where ϕ_1 (ϕ_2) is the positional phase of vortex 1 (2). For the case of the two same-polarity vortices [Fig. 7(e)] we see a striking pattern. As energy is transferred from vortex 1 to vortex 2, the relative phase is negative with an amplitude of around unity. When the energy transfer reverses, we see a sudden switch in the relative phase, which becomes positive and again of amplitude of around unity. This phase pattern repeats in synchrony with the energy transfer. If we consider the high energy vortex (during any given transfer period) to be the "driving" vortex, we see that energy is driven into the other vortex when the "driver" lags the vortex by approximately a unit phase. This is indicative of strong coupling between the vortices, which we attribute to sound waves. This observation will become important in the next section when we mimic the driving vortex by a moving obstacle.

In comparison, when the vortices are of opposite polarity, the phase difference accrues with time and suggests no such coupling exists between the vortices (i.e., the vortices evolve largely independently).

While it would appear that the vortices periodically drive energy into each other via their emitted sound, we must rule out that this effect arises from the long-range interaction between vortices due to their superimposed velocity fields. To this aim, we will next attempt to drive a vortex via sound waves generated by artificial means—a moving localized barrier.

V. PRECESSING OBSTACLE

We return to having one vortex in the system, in the right-hand well, but now consider a localized obstacle precessing in the left-hand well. We continue to employ the idealized double harmonic trap; the same effects will be demonstrated in an experimentally realizable trap in Sec. VII. The obstacle corresponds to a Gaussian potential,

$$V_{\rm ob}(x,y,t) = A_{\rm ob}\exp\left[-\frac{\{x+x_c-x_{\rm ob}(t)\}^2+\{y-y_{\rm ob}(t)\}^2}{\sigma^2}\right], \tag{4}$$

with time-dependent location $(x_{\rm ob}(t),\ y_{\rm ob}(t))$, amplitude $A_{\rm ob}$ and width σ. Such a moving Gaussian obstacle can be induced experimentally by the presence of a blue-detuned laser beam [9,40].

A. Regular circular precession

We first consider the simplest case where the obstacle undergoes regular circular motion, with constant radius $r_{\rm ob}$ and angular frequency $\omega_{\rm ob}$. The motion is either co-rotating or antirotating with respect to the vortex. Specifically, the obstacle coordinates are $x_{\rm ob}(t) = \pm r_{\rm ob}\sin\omega_{\rm ob}t$ and $y_{\rm ob}(t) = r_{\rm ob}\cos\omega_{\rm ob}t$.

We generate sound that mimics the sound generated by a vortex and so employ precession frequencies similar to the vortex precession frequency ($\sim 0.23\omega$ for the condensate system employed here). Such motion is sufficiently slow to avoid exceeding the superfluid critical velocity and nucleating vortices [9,40–42]. Simulations confirm that the only excitations generated by the obstacle are spiral sound waves with typical amplitude $\sim 1\% n_0$.

Under the influence of such an obstacle, typical vortex dynamics are presented in Fig. 8. When the barrier moves in the same direction as the vortex (solid black line in Fig. 8), the vortex radial position oscillates in time, demonstrating a

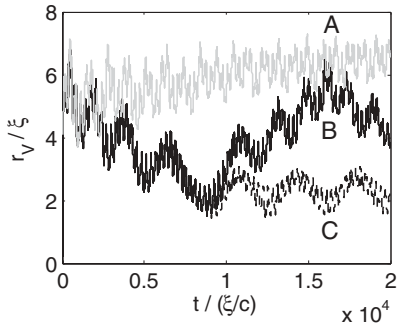

FIG. 8. Evolution of the vortex radius under the influence of an obstacle undergoing constant-speed circular motion. [Light gray line (A)] The obstacle moves in the opposite direction to the vortex. [Black line (B)] The obstacle moves in the same direction as the vortex. [Dashed line (C)] The barrier moves in the same direction as the vortex but its motion is terminated at $t = 8800(\xi/c)$. Parameters are as follows: $r_1(t=0) = 4\xi, \sigma = 2\xi, r_{ob} = 4\xi, \phi_{ob} = 0$, and $\omega_{ob} = 0.234\omega$ and $V_0 = 0.6\mu$.

periodic driving of energy into the vortex. Conversely, if the barrier moves in the opposite direction to the vortex (gray line) no driving is observed (although a small outward shift of the vortex suggests a small loss of energy in this case). These results show the same qualitative behavior as observed earlier when a vortex is driven by another vortex.

Terminating the obstacle motion leads to a vortex which maintains a roughly constant radius and energy (dotted black line in Fig. 8). In this manner we can parametrically drive net energy into the vortex.

Taking the minimum radius achieved r_{min} as a measure of the driving effectiveness, we demonstrate the driving effectiveness as a function of the obstacle parameters ω_{ob}, A_{ob}, and σ in Fig. 9. For each case there exists a clear resonance that maximizes the energy that can be driven into the vortex. Driving is most effective when the obstacle most closely mimics a vortex, that is, has a precession frequency close to that of a vortex and a width and amplitude that generates a vortexlike perturbation in the density. Furthermore, when the obstacle moves in the opposite direction to the vortex, no

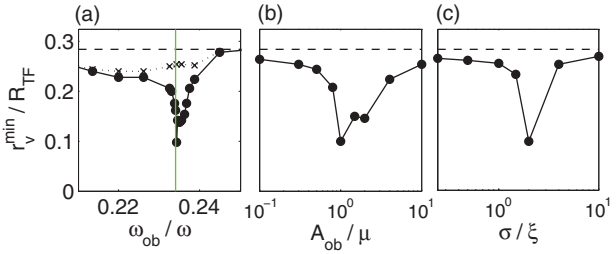

FIG. 9. (Color online) Minimum radial position achieved by the vortex, initially at $r_v = 4\xi$ (dashed line), under the influence of a precessing Gaussian barrier during a total simulation time of $2 \times 10^4(\xi/c)$. Unless it is the abcissa, the obstacle parameters are as follows: $\omega_{ob} = 0.234\omega$, $A_{ob} = \mu$, $\sigma = 2\xi$, and $r_{ob} = 4\xi$. In (a) we present results for co-rotating (solid line with dots) and antirotating (dashed line with crosses) system. In (b) and (c) we consider only the co-rotating system. In (a) we show the precession frequency of the undriven vortex [green (gray) vertical line].

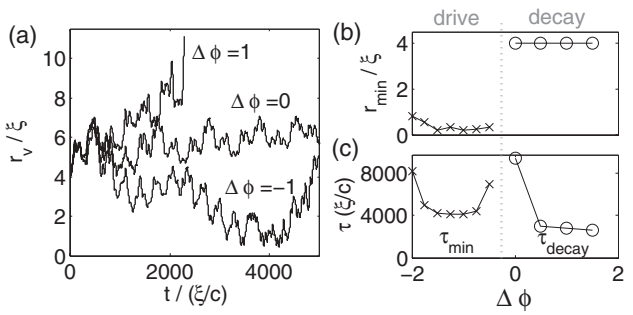

FIG. 10. (a) Evolution of the vortex radial position under the influence of a precessing obstacle with fixed relative phase $\Delta\phi = -1$, 0 and -1. (b) Minimum radial position achieved as a function of relative phase. (c) Time scale of the vortex dynamics τ, either the time to reach the minimum radial position τ_{min} or decay out of the condensate τ_{decay}. The remaining obstacle parameters are $A_{ob} = \mu$, $\sigma = 2\xi$, and $r_{ob} = 6\xi$.

resonance in driving appears. For this reason, we subsequently only consider the co-rotating case.

While the phase difference between the vortex and the obstacle varies with time, the cycling of the vortex in or out corresponds to when the obstacle lags or leads the vortex, consistent with the phase behavior for two vortices discussed in Sec. IV. We will exploit the phase relationship in the following subsection.

B. Vortex-dependent precession

In Sec. IV we saw that successful driving of one vortex by another coincided with when the phase of the "driver" lagged that of the "receiver" by a phase of around unity. Motivated by this, we next implement a driving scheme in which the obstacle is forced to have a constant phase offset from the vortex $\Delta\phi$. The time-dependent obstacle coordinates become

$$x_{ob}(t) = r_v(t)\cos[\phi_v(t) + \Delta\phi],$$
$$y_{ob}(t) = r_v(t)\sin[\phi_v(t) + \Delta\phi],$$

where $r_v(t) = \sqrt{x_v^2(t) + y_v^2(t)}$ is the radial position of the vortex and $\phi_v(t) = \arctan(y_v(t)/x_v(t)$ its phase angle, relative to the center of its respective well. We use the same obstacle height and width as above ($A_{ob} = \mu$ and $\sigma = 2\xi$).

Typical results are shown in Fig. 10. When the obstacle is in phase ($\Delta\phi = 0$) or leads ($\Delta\phi > 0$) the vortex, the vortex drifts outwards. However, when the obstacle lags the vortex ($\Delta\phi < 0$), the vortex is driven towards the trap center, increasing its energy. Under optimal conditions, the vortex is driven into the trap center within a time scale of $4000(\xi/c)$, significantly quicker than we observed for constant obstacle precession frequency.

The relative phase controls whether the vortex decays (moves outwards) or is driven (moves inwards), and also the time scale over which this occurs (defined either by the time scale to reach the minimum radius τ_{min} or decay out of the condensate τ_{decay}), as mapped out in Figs. 10(b) and 10(c). The most rapid driving of the vortex occurs when the obstacle lags the vortex by approximately a unit phase. *Nota bene* we found exactly these optimum phase differences to naturally arise in the two-vortex system [see Fig. 7(e)].

VI. DISCUSSION

A. Crossover and induction dynamics

Our precursive study of a single vortex in an idealized double trap has demonstrated "crossover" and "inductive" regimes. The latter case effectively provides a physical manifestation of "mirror" vortices. While these states are transient, they can exist for significant time scales, for example, several periods of vortex precession. The generation of a vortex state across a double-well system has been studied in [43]. However, there the vortex-containing BEC partially tunneled into the adjacent empty well, and so is a distinct creation mechanism to the one observed here.

B. Origin of the vortex coupling

Our main results show cycling of the energy or radial position between two vortices, each located in one well. We have interpreted this as being due to the exchange of sound waves between the vortices. An alternative origin is that the vortex coupling arises from the interaction between vortices as a result of their velocity fields, for example, as plays a central role in Tkachenko oscillations of a vortex lattice [54,55] and the dynamics of vortex dipoles [52,53], clusters [56], and arrays [57]. First, the velocity field-induced vortex-vortex interaction is weak due to the separation of the vortices in weakly connected subsystems (a reduction of density near a boundary has been shown to dramatically reduce this type of vortex-vortex interaction [60]). Secondly, if the vortex-vortex interaction were driving the coupled dynamics, we would expect the vortices to follow lines of equipotential formed by contributions from the trapping potential and the vortex-vortex interaction. This is not the case in the observed dynamics, for which the intervortex distances oscillates rapidly while the vortex radial position undergoes a much slower oscillation. Thirdly, and most importantly, we observe the same physical effect when the vortex-vortex interaction is removed altogether (i.e., one vortex driven by a sound-generating obstacle).

A further alternative explanation is that the system acts as a coherent superposition of a vortex-less ground state and two collective vortex modes, with the dynamics arising from a coherent beating between these excitations. Again, the observation of vortex driving via an obstacle would seem to contradict this picture.

Based on these arguments, we believe that the vortex cycling is due to the exchange of energy via sound waves.

C. Cross talk between vortices

When the two vortices have the same polarity and different initial positions and energies, they undergo periodic exchanges of energy with each other, transferred via sound waves. We may view this as the driving of a vortex by sound from another vortex. The transfer of energy occurs rapidly, with a full energy cycle typically occurring within 10 vortex precessions. The relative phase between the vortices appears intimately linked to the exchange of energy, alternating in line with the direction of energy transfer.

The sound is emitted from the accelerating vortex in the form of a quadrupolar radiation pattern [23]. The precession of the vortex in the trap leads to an outward-propagating spiral wave of sound. This sound carries angular momentum of the same orientation as the originating vortex (to conserve angular momentum). If the angular momentum carried by the sound waves is of the same orientation as the receiving vortex (which is to say that the vortices are of the same polarity), it serves to increase the angular momentum and energy of this vortex, causing it to move towards the high density trap center. By the reverse argument, one would expect that when the vortices are of opposite polarity, the receiving vortex would have its energy and angular momentum reduced. However, in this case, the vortices have negligible effect on each other (we will return to this anomaly later).

The cross talk between vortices is analogous to that predicted for dark solitons in a double well [34]. However, there the energy transfer occurred over a much longer time scale, corresponding to many tens of oscillations.

D. Parametric driving of a vortex

By moving a localized obstacle through one well, we generate angular-momentum carrying sound waves. For suitable obstacle parameters, these sound waves drive energy into a vortex located in the opposite well. This process is most effective when the time-dependent density perturbation created by the obstacle closely matches that of the vortex (i.e., the same width, precession frequency, and amplitude). Similar to above, transfer of energy from sound into the vortex only occurs when the obstacle-induced sound and the vortex have the same sign of angular momentum.

When the obstacle undergoes uniform circular motion, the transfer of energy is somewhat slow. More rapid driving of the vortex occurs when the phase of the obstacle motion is forced to *lag* behind the vortex motion. This suggests that the relative phase between the vortex and incident sound waves is crucial in controlling the absorption of sound by the vortex.

In Ref. [44] a driving obstacle and vortex resided in the same trap. There the precessing obstacle periodically formed a vortex at the condensate edge and drove it into the center, interpreted as nonlinear Rabi cycling from the ground state to the first vortex state. Similarly, we may interpret our observations as oscillations between a high- and low-energy vortex state. Moreover, our results suggest that sound waves may have played a central role in transferring energy from the obstacle to the vortex.

An analogous driving technique has been demonstrated for a dark soliton in a trapped BEC [20]. Oscillating paddles generate sound waves and a dipole moment of the condensate, which deposit some of their energy to the dark soliton. Similarly to our observations, optimum driving occurred when the driving frequency approximated the unperturbed soliton frequency and for strict phase relations between the drive and soliton.

E. Insight into sound absorption in trapped and homogeneous systems

Using an acoustic ray model, Nazarenko *et al.* [26,27] find that certain trajectories of the sound waves incident on a vortex line can spiral into the vortex core, imparting their energy. Despite this, sound absorption is not cited to play

a significant role in superfluid helium systems, for example, quantum turbulence [2,3].

Consider an element of vortex line in an infinite homogeneous system emitting a pulse of sound. The pulse could in principle impart energy into a neighboring line element of matching angular momentum. However, from the point of emission, the sound spreads radially outwards, diluting its energy and angular momentum density. Superimpose many such events from many randomly oriented vortex lines and the combined sound field will be highly isotropic with no net angular momentum, incapable of causing any significant net sound absorption.

Now consider a trapped BEC, for example, the double trap employed here. An outward spreading sound pulse will eventually reflect off the trap wall, partially focusing the wave towards the trap center. While the exact effectiveness of the focusing will vary with source position and trap shape, it will nonetheless lead to a greater and more sustained sonic angular momentum and energy density than in a homogeneous system, which a suitably placed vortex may be able to gain from. The focusing of the emitted sound pulse will, however, be short-lived since the sonic angular momentum will become randomized after several reflections. Indeed, we see this effect in Fig. 4 where a sound pulse, initially with net momentum, becomes rapidly randomized into an isotropic sound field. The rapid randomization of sound also explains the rapid equilibrium reached in the vortex position or energy when the driving obstacle is suddenly made stationary. Sound absorption is thus likely to play a much more significant role in trapped condensates than in homogeneous systems.

Irrespective of the source of the sound, we observe transfer of energy between sound and vortex only when the angular momentum of the sound and the vortex have the same orientation. Within the Nazarenko picture [26,27] only trajectories of sound which spiral into the vortex core can impart energy and angular momentum to the vortex. When the sound waves have the same angular momentum as the vortex, they naturally wrap around the vortex, allowing them to spiral into the core and interact with the vortex. Conversely, when the sound has opposite angular momentum to the vortex, the sound will tend to be deflected by the vortex; in essence, the vortex is then invisible to sound waves of opposite angular momentum.

In our disk-shaped quasi-2D system, the vortex line is rectilinear and can only raise its energy by moving to regions of higher density (increasing the kinetic energy density of the flow). In a 3D system, the vortex can additionally absorb energy by increasing its line length or developing line excitations. The favored channel has not been studied but is likely to depend strongly on the distribution and orientation of the incident sound.

VII. PROPOSED EXPERIMENTAL REALIZATION

The double trap used thus far [defined by Eq. (2)] is not experimentally realizable. Here we will demonstrate that the same qualitative phenomena occur in experimentally realizable traps. We approximate the double harmonic trap (2) by a single elliptical harmonic trap split by a central Gaussian barrier lying along the y axis, that is,

$$V(x,y) = \frac{m}{2}\left[\frac{\omega^2 x^2}{4} + \omega^2 y^2\right] + V_{\rm B} e^{-x^2/2d^2} - V_{\rm min}, \quad (5)$$

where

$$V_{\rm min} = -m\omega^2 d^2\left[\ln\frac{V_{\rm B}}{m\omega^2 d^2} + 1\right] \quad (6)$$

is an offset such that the potential minimum is zero. Then the height of the barrier is $V_0 = V_{\rm B} - V_{\rm min}$. For a barrier width $d = 5\xi$ the split trap well approximates the double harmonic trap as shown in Fig. 11. Assuming typical parameters (a 2D peak density $n_0 = 10^{14}{\rm m}^{-2}$, $\omega_z = 2\pi \times 1000$ Hz, and $\omega = 2\pi \times 50$ Hz), then for a ^{87}Rb (^{23}Na) BEC, the healing length is $\xi = 0.3(0.7)\mu$m, the speed of sound $c = 3(4)$mms^{-1}, and the time unit $(\xi/c) = 90(175)\mu$s.

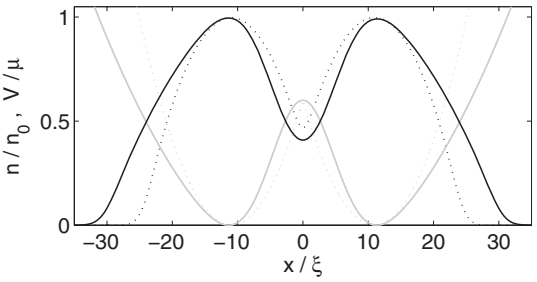

FIG. 11. The split trap potential (gray solid line) and idealized double harmonic potential (gray dotted line), and their corresponding density profiles (black lines), all shown along the y axis and satisfying $\mu = 10\hbar\omega$.

A. Cross talk of two vortices

The wells are no longer circularly symmetric and so we specify the y displacement of the vortices rather than their radial displacement. The stability diagrams for one and two vortices in the split trap, shown in Fig. 12, are in close agreement with the corresponding plots for the double

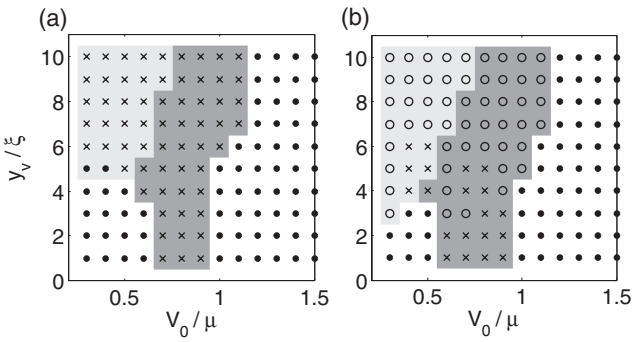

FIG. 12. Stability diagrams for the vortex dynamics in a split trap as a function of vortex displacement y_v and barrier height V_0. (a) A single vortex in the right-hand well. Solid circles (crosses) correspond to the final state [after 5000 (ξ/c)] being a vortex (vortex-free) state. (b) A vortex in each well, of the same polarity. The final state is either two stable vortices (solid circles), one stable vortex (open circles), or no vortices (crosses). In both (a) and (b) the light-shaded (dark-shaded) region corresponds to case I (II) of the vortex dynamics.

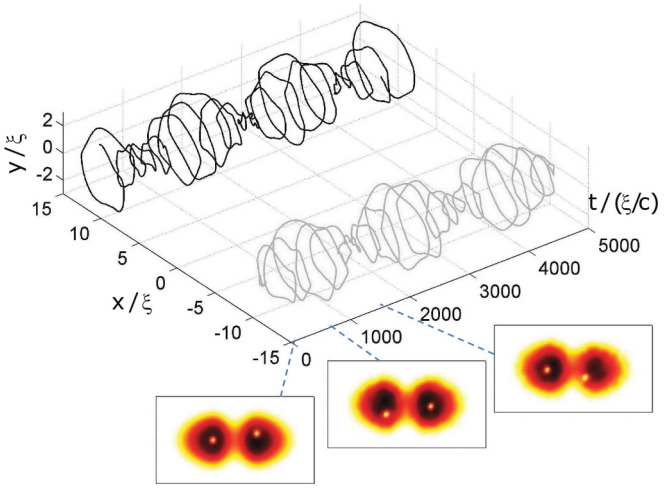

FIG. 13. (Color online) Vortex motion during cross talk in the split trap. Also shown are plots of the BEC density at $t = 0$, 850, and 1550 (ξ/c). The vortices move anticlockwise. In the color-density mapping black corresponds to high density while white corresponds to zero density. Parameters are $V_0 = 0.5\mu$ and $y_v = 3\xi$.

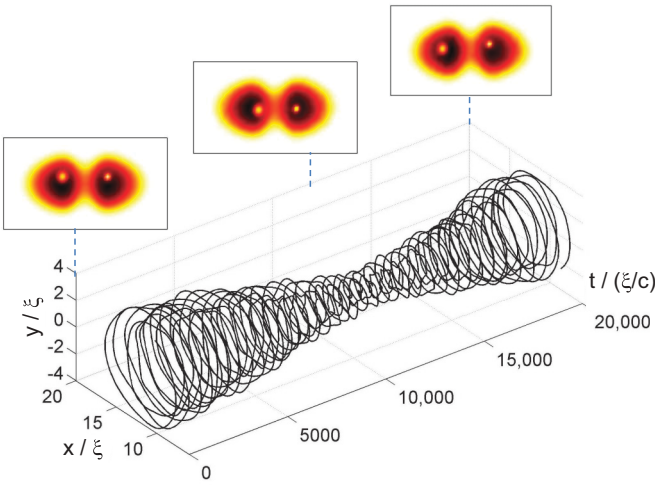

FIG. 14. (Color online) Vortex motion under parametric driving by a precessing obstacle in the split trap. The BEC density is presented at $t = 0$, 12 000, and 20 000 (ξ/c). The obstacle (left well) and the vortex (right well) move anticlockwise. Parameters are $y_v(t = 0) = 3\xi$, $V_0 = 0.5\mu$, $\sigma = 2\xi$, $A_{\rm ob} = \mu$, $y_{\rm ob} = 3\xi$, and $\omega_{\rm ob} = 0.234\omega$.

harmonic trap [Figs. 2 and 6(a)] and demonstrate the same crossover and inductive dynamics.

Focusing on a stable case from the two-vortex system ($y_v = 3\xi$ and $V_0 = 0.5\mu$), we show the evolution of the vortices in Fig. 13. The vortices drift in and out of the trap center, out of phase with each other, in agreement with the energy transfer observed earlier in Fig. 7(a). The period of the energy transfer is around $1600(\xi/c)$ or eight vortex precessions. Snapshots of the condensate density show the initial appearance of the condensate (vortex 1 at large radius and vortex 2 at the trap center), after a half-cycle of energy exchange (vortex 1 at the trap center and vortex 2 at large radius) and after a full cycle of energy exchange (vortex 1 returns to large radius and vortex 2 returns to the trap center).

B. Precessing obstacle

The addition of a precessing Gaussian obstacle to a harmonic trap has been demonstrated experimentally [9,40]. We employ obstacle parameters $\sigma = 2\xi$, $A_{\rm ob} = \mu$, $y_{\rm ob} = 3\xi$, $\phi_{\rm ob} = 0$, and $\omega_{\rm ob} = 0.234\omega$. Here we consider constant frequency precession of the obstacle; the "phase-locked" method of Sec. V B requires real-time feedback of the vortex position and is not experimentally feasible at present. Under such a perturbation within the split trap (Fig. 14) the vortex becomes driven into the trap center, in close agreement with the dynamics in the idealized trap (Fig. 8). The same resonant behavior as Fig. 9 is also observed in the split trap, for example, a frequency resonance when $\omega_{\rm ob}$ approaches the precession frequency of the unperturbed vortex ($\sim 0.234\omega$).

C. Experimental observation

The vortex-vortex and vortex-obstacle energy transfer could be observed through the motion of the vortices in and out of the trap center. Recently, Freilich *et al.* [13] demonstrate real-time tracking of vortices in a BEC. This involves transferring (via pulsed microwave radiation) a small, representative proportion of the BEC into an untrapped state, which is allowed to expand and then imaged via optical absorption. This is repeated at regular time intervals to enable the vortex motion to be tracked. For ^{87}Rb (^{23}Na) the energy exchange period for the vortex-vortex case we consider is $\sim$0.15(0.3)s, while for the vortex-obstacle case it is $\sim$1.8(3.5)s. These time scales are well within the experimental lifetime of vortices in BECs (up to $\sim$10 s [7]).

VIII. CONCLUSION

We have shown that two vortices in a double-well trap can undergo coherent crosstalk, exchanging energy and angular momentum with each other. This interaction is mediated by sound waves which are emitted from each vortex due to their acceleration and impart their energy and angular momentum onto the other vortex. These observations are strongly analogous to the sound-mediated interactions between matter-wave dark solitons, where interaction occurs through linear-momentum-carrying sound waves. This further evidences the striking similarities in the acoustic behavior of vortices and dark solitons. An analogous transfer of energy into a vortex can be achieved by sound waves generated by a precessing obstacle. Such pumping could, for instance, be exploited to counteract thermal decay and extend vortex lifetimes. Crucially, for the sound energy to be driven into the vortex, first, the sound must carry angular momentum of the same sign as the vortex and, secondly, the motion of the "driver" (be it an obstacle or another vortex) should *lag* the motion of the target vortex.

Our observations are robust: We observe the same qualitative dynamics for different condensate parameters (e.g., a large, more Thomas-Fermi condensate). Importantly, these effects occur in experimentally realizable double-well geometries and within the time scales of both current vortex experiments and thermal decay [45,46,58,59].

Sound absorption is promoted by the trapped nature of the BEC systems and is likely to play a much more significant role than in homogeneous superfluids. An example may lie in the formation of vortex lattices in rotating BECs whereby nucleated vortices are observed to crystallize into a vortex lattice. While the necessary dissipation is provided by thermal decay at raised temperatures [47–49], crystallization at very low temperatures has been show to be temperature independent [50]. Here, vortex-sound interactions may play the key role, enabling energy exchange between vortices and the sound field [51].

Improved understanding of the rudimentary interactions between quantum vortices and sound will aid in resolving their role in wider phenomena such as quantum turbulence [3] and neutron star glitches [61].

ACKNOWLEDGMENTS

We acknowledge funding from the United Kingdom Engineering and Physical Sciences Research Council (Grant No. EP/I019413/1) and thank the anonymous referee for constructive comments.

[1] R. J. Donnelly, *Quantized Vortices in Helium II* (Cambridge University Press, Cambridge, 1991).
[2] C. F. Barenghi, R. J. Donnelly, and W. F. Vinen (eds.), *Quantized Vortex Dynamics and Superfluid Turbulence* (Springer, Berlin, 2001).
[3] W. F. Vinen, J. Low Temp Phys. **161**, 419 (2010).
[4] A. L. Fetter and A. A. Svidzinsky, J. Phys.: Condens. Matter **13**, R135 (2001).
[5] B. P. Anderson, J. Low Temp. Phys. **161**, 574 (2010).
[6] M. R. Matthews, B. P. Anderson, P. C. Haljan, D. S. Hall, C. E. Wieman, and E. A. Cornell, Phys. Rev. Lett. **83**, 2498 (1999).
[7] P. Rosenbusch, V. Bretin, and J. Dalibard, Phys. Rev. Lett. **89**, 200403 (2002).
[8] P. Engels, I. Coddington, P. C. Haljan, V. Schweikhard, and E. A. Cornell, Phys. Rev. Lett. **90**, 170405 (2003).
[9] T. W. Neely, E. C. Samson, A. S. Bradley, M. J. Davis, and B. P. Anderson, Phys. Rev. Lett. **104**, 160401 (2010).
[10] N. S. Ginsberg, J. Brand, and L. V. Hau, Phys. Rev. Lett. **94**, 040403 (2005).
[11] E. A. L. Henn, J. A. Seman, G. Roati, K. M. F. Magalhães, and V. S. Bagnato, Phys. Rev. Lett. **103**, 045301 (2009).
[12] G. P. Bewley, D. P. Lathrop, and K. R. Sreenivasan, Nature (London) **441**, 588 (2006).
[13] D. V. Freilich, D. M. Bianchi, A. M. Kaufman, T. K. Langin, and D. S. Hall, Science **3**, 1182 (2010).
[14] O. Bühler, Annu. Rev. Fluid Mech. **42**, 205 (2010).
[15] This is well established within a uniform condensate, particularly for superfluid helium [3]. However, under conditions of a trapped, three-dimensional condensate under rotation, the lowest Kelvin mode has been predicted to become the lowest frequency mode of the system [16].
[16] T. P. Simula, T. Mizushima, and K. Machida, Phys. Rev. Lett. **101**, 020402 (2008).
[17] M. Leadbeater, T. Winiecki, D. C. Samuels, C. F. Barenghi, and C. S. Adams, Phys. Rev. Lett. **86**, 1410 (2001).
[18] E. Lundh and P. Ao, Phys. Rev. A **61**, 063612 (2000).
[19] W. F. Vinen, Phys. Rev. B **64**, 134520 (2001).
[20] N. P. Proukakis, N. G. Parker, C. F. Barenghi, and C. S. Adams, Phys. Rev. Lett. **93**, 130408 (2004).
[21] C. F. Barenghi, N. Parker, N. Proukakis, and C. Adams, J. Low Temp. Phys. **138**, 629 (2005).
[22] M. Leadbeater, D. C. Samuels, C. F. Barenghi, and C. S. Adams, Phys. Rev. A **67**, 015601 (2003).
[23] N. G. Parker, N. P. Proukakis, C. F. Barenghi, and C. S. Adams, Phys. Rev. Lett. **92**, 160403 (2004).
[24] S. I. Davis, P. C. Hendry, and P. V. E. McClintock, Physica B (Amsterdam) **280**, 43 (2000).
[25] P. M. Walmsley, A. I. Golov, H. E. Hall, A. A. Levchenko, and W. F. Vinen, Phys. Rev. Lett. **99**, 265302 (2007).
[26] S. V. Nazarenko, Phys. Rev. Lett. **73**, 1793 (1994).
[27] S. V. Nazarenko, N. J. Zabusky, and T. Scheidegger, Phys. Fluids **7**, 2407 (1995).
[28] K. W. Schwarz and C. W. Smith, Phys. Lett. A **82**, 251 (1981).
[29] N. G. Berloff and C. F. Barenghi, Phys. Rev. Lett. **93**, 090401 (2004).
[30] P. G. Kevrekidis, R. Carretero-Gonzalez, G. Theocharis, D. J. Frantzeskakis, and B. A. Malomed, J. Phys. B **36**, 3467 (2003).
[31] Th. Busch and J. R. Anglin, Phys. Rev. Lett. **84**, 2298 (2000).
[32] N. G. Parker, N. P. Proukakis, and C. S. Adams, Phys. Rev. A **81**, 033606 (2010).
[33] N. G. Parker, N. P. Proukakis, M. Leadbeater, and C. S. Adams, Phys. Rev. Lett. **90**, 220401 (2003).
[34] A. J. Allen, D. P. Jackson, C. F. Barenghi, and N. P. Proukakis, Phys. Rev. A **83**, 013613 (2011).
[35] C. J. Pethick and H. Smith, *Bose-Einstein Condensation in Dilute Gases* (University Press, Cambridge, 2002).
[36] By "decay" we refer to the loss of energy from the vortex excitation, not from the system as a whole.
[37] A. Minguzzi, S. Succi, F. Toschi, M. P. Tosi, and P. Vignolo, Phys. Rep. **395**, 223 (2004).
[38] D. S. Rokhsar, Phys. Rev. Lett. **79**, 2164 (1997).
[39] A. A. Svidzinsky and A. L. Fetter, Phys. Rev. A **62**, 063617 (2000).
[40] C. Raman, J. R. Abo-Shaeer, J. M. Vogels, K. Xu, and W. Ketterle, Phys. Rev. Lett. **87**, 210402 (2001).
[41] B. Jackson, J. F. McCann, and C. S. Adams, Phys. Rev. A **61**, 051603(R) (2000).
[42] R. Onofrio, C. Raman, J. M. Vogels, J. R. Abo-Shaeer, A. P. Chikkatur, and W. Ketterle, Phys. Rev. Lett. **85**, 2228 (2000).
[43] J. R. Salgueiro, M. Zacarés, H. Michinel, and A. Ferrando, Phys. Rev. A **79**, 033625 (2009).
[44] B. M. Caradoc-Davies, R. J. Ballagh, and K. Burnett, Phys. Rev. Lett. **83**, 895 (1999).
[45] P. O. Fedichev and G. V. Shlyapnikov, Phys. Rev. A **60**, R1779 (1999).

[46] B. Jackson, N. P. Proukakis, C. F. Barenghi, and E. Zaremba, Phys. Rev. A **79**, 053615 (2009).
[47] C. Lobo, A. Sinatra, and Y. Castin, Phys. Rev. Lett. **92**, 020403 (2004).
[48] A. A. Penckwitt, R. J. Ballagh, and C. W. Gardiner, Phys. Rev. Lett. **89**, 260402 (2002).
[49] M. Tsubota, K. Kasamatsu, and M. Ueda, Phys. Rev. A **65**, 023603 (2002).
[50] J. R. Abo-Shaeer, C. Raman, and W. Ketterle, Phys. Rev. Lett. **88**, 070409 (2002).
[51] N. G. Parker and C. S. Adams, Phys. Rev. Lett. **95**, 145301 (2005); J. Phys. B **39**, 43 (2006).
[52] S. Middelkamp, P. J. Torres, P. G. Kevrekidis, D. J. Frantzeskakis, R. Carretero-Gonzalez, P. Schmelcher, D. V. Freilich, and D. S. Hall, Phys. Rev. A **84**, 011605(R)(2011).
[53] P. J. Torres, P. G. Kevrekidis, D. J. Frantzeskakis, R. Carretero-Gonzlez, P. Schmelcher, and D. S. Hall, Phys. Lett. A **375**, 3044 (2011).
[54] I. Coddington, P. Engels, V. Schweikhard, and E. A. Cornell, Phys. Rev. Lett. **91**, 100402 (2003).
[55] T. Mizushima, Y. Kawaguchi, K. Machida, T. Ohmi, T. Isoshima, and M. M. Salomaa, Phys. Rev. Lett. **92**, 060407 (2004).
[56] V. Pietila, M. Mottonen, T. Isoshima, J. A. M. Huhtamaki, and S. M. M. Virtanen, Phys. Rev. A **74**, 023603 (2006).
[57] T. P. Simula and K. Machida, Phys. Rev. A **82**, 063627 (2010).
[58] S. J. Rooney, A. S. Bradley, and P. B. Blakie, Phys. Rev. A **81**, 023630 (2010).
[59] S. J. Rooney, P. B. Blakie, B. P. Anderson, and A. S. Bradley, Phys. Rev. A **84**, 023637 (2011).
[60] P. Mason and N. G. Berloff, Phys. Rev. A **77**, 032107 (2008).
[61] L. Warszawski, A. Melatos, and N. G. Berloff, Phys. Rev. B **85**, 104503 (2012).